Symmetric Training Sequence-Based Carrier Frequency Offset Estimation Scheme for Coherent Free-Space Optical Communication

Xinyu Tang, Liqian Wang, Shanyong Cai, Qin Mei, and Zhiguo Zhang

***Abstract*—In this paper, a symmetric training sequence-based (STSB) carrier frequency offset estimation (FOE) scheme for coherent free-space optical (CFSO) communication is proposed. In the proposed technique, we exploit the training-sequence-based (TSB) carrier FOE algorithm to the CFSO communication system in the quadrature phase-shift keying (QPSK) modulation format. A symmetric training sequence, tailored to the carrier FOE algorithm for atmospheric turbulence channel, is formulated to accurately identify the correct temporal position of a data frame from received signals. Unlike the 4th power algorithm, the proposed algorithm requires only the identified training sequence and the symmetric sequence of the original training sequence in the FOE stage, performing a single multiplication to accurately remove the signal modulation phase. In this way, the proposed technique significantly improves the estimation accuracy. Furthermore, by avoiding the time-consuming 4th power operation, the proposed method reduces the computational complexity while expanding the FOE range. Therefore, when compared with existing algorithms, our proposed technique can achieve more accurate timing, a wider estimation range, and lower complexity. A 10-Gbps QPSK CFSO communication transmission experiment with different turbulence channels was carried out to validate the proposed technique and the improvement in receiver sensitivity.**

***Index Terms*—Coherent free-space optical communication, carrier frequency offset estimation, digital signal processing, training sequence, turbulence.**

I. Introduction

With the development of space technology, the requirements for information capacity and transmission speed have considerably increased. In this context, free-space optical (FSO) communication technology has become a popular research direction in the field of optical communication due to its large capacity, high bandwidth, and high confidentiality [1]–[4]. There are two reception detection methods: intensity modulation direct detection (IM/DD) [5], [6] and coherent detection [7], [8]. Most IM/DD communication systems use binary on-off keying (OOK) modulation [9], [10]. This system is widely used in low-rate and short-distance communication transmission systems due to its technological maturity, low cost and simple structure. Compared with the IM/DD detection method, the coherent detection method is more flexible in terms of modulation. In addition to intensity modulation, it can modulate the frequency and phase of optical waves. Coherent communication systems are critical in the field of next-generation FSO communication [11]–[14]. To achieve high-speed, high-capacity information transmission systems, coherent detection systems combined with high-order modulation technology have become an attractive modulation scheme [15], [16].

The atmospheric link channel condition has a considerable impact on the performance of coherent free-space optical (CFSO) communication systems. Due to the temporal variability of atmospheric turbulence, the atmospheric refractive index fluctuates, causing wave front distortions in the optical signal, resulting in signal power attenuation and phase distortion [17]–[20]. Using digital coherent reception (DCR) technology, the received signal can be frequency offset estimated and phase-compensated at the receiver side using digital signal processing (DSP) algorithms, thus reducing the bit-error rate (BER) of the system [21]. Current carrier frequency offset estimation (FOE) algorithms in DCR technology can be broadly classified into two categories: frequency domain FOE algorithms and time domain FOE algorithms. The Fast Fourier Transform (FFT) based frequency domain FOE algorithm [22], [23] needs to be converted to the frequency domain for spectrum analysis in the FOE stage to determine the carrier FOE. The estimation accuracy of this method was limited by the spectral resolution, and greatly increases the complexity of the field-programmable gate array (FPGA) implementation. Compared with the FFT algorithm, the time domain FOE algorithm does not require frequency domain variation, so it can obtain lower computational complexity.

In the time domain FOE algorithm, the classical 4th power algorithm [24] uses the 4th power function to remove the received signal modulation phase, resulting in a FOE with low accuracy and a small estimation range. Based on the 4th algorithm, a training sequence-based (TSB) time domain FOE algorithm was proposed in [25]. The TSB algorithm was based on the idea of Schmidl & Cox's (S&C) algorithm [25] and used a frame

Manuscript received January 27, 2022; revised March 2, 2022; accepted March 19, 2022. Date of publication March 23, 2022; date of current version April 21, 2022. This work was supported by the National Natural Science Foundation of China under Grant 62075017. *(Corresponding author: Liqian Wang.)*

Xinyu Tang, Liqian Wang, Shanyong Cai, and Zhiguo Zhang are with the State Key Laboratory of Information Photonics and Optical Communications, Beijing University of Posts and Telecommunications, Beijing 100876, China (e-mail: tangxinyu@bupt.edu.cn; lqwangwang@bupt.edu.cn; caishanyong@bupt.edu.cn; zhangzhiguo@bupt.edu.cn).

Qin Mei is with the Wuxi Electric Power Supply Company, Wuxi 314061, China (e-mail: 13585085089@126.com).

Digital Object Identifier 10.1109/JPHOT.2022.3161795

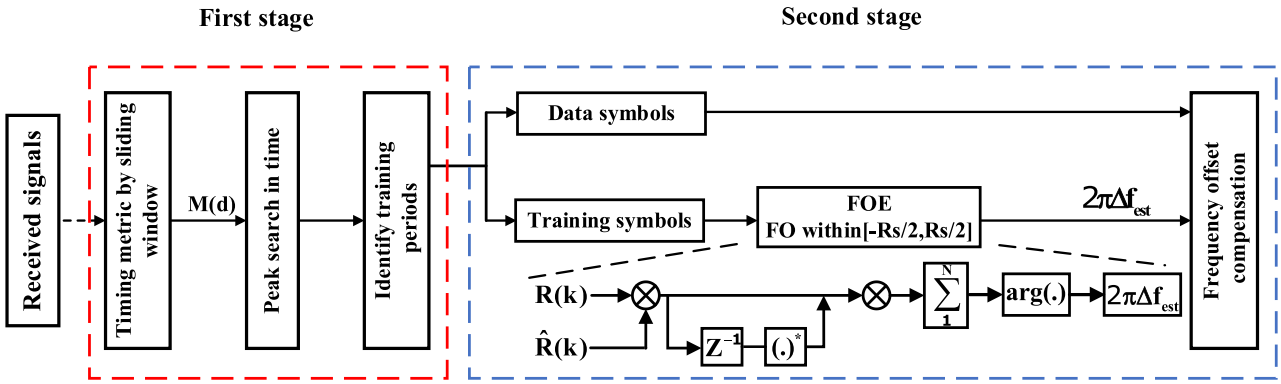

Fig. 1. Block diagram of the proposed scheme.

synchronization algorithm to determine the start point of each training period frame in the received sequence to extract the timing training sequence for FOE. In addition, the training sequence was placed at the beginning of each data frame or was inserted periodically. Hence, it is essential to correctly identify timing these training sequences. The S&C algorithm uses a training sequence with two identical pseudo-noise (PN) sequences for frame synchronization. However, its timing metric plateaus at the highest correlation point, resulting in a considerable error in timing synchronization at worse channels and thus inaccurate estimation in the subsequent FOE stage.

The development of an efficient and accurate algorithm with low complexity for CFSO communication systems is a challenging task. The existing methods cannot solve this problem efficiently. In this article, we propose a symmetric training sequence-based (STSB) carrier FOE scheme for the CFSO system. With the proposed technique, we can achieve more accurate timing, a wider estimation range, and lower complexity. Due to the optimized structure of the training sequence, high-precision timing synchronization can be achieved even at lower optical transmitting powers. In addition, by performing a single multiplication operation in the carrier FOE stage using the identified training sequence and the symmetric sequence of the original training sequence, the modulated phase of the received signal can be accurately removed, allowing the FOE range of [-symbol rate/2, +symbol rate/2] to be realized. The effectiveness and feasibility of this scheme were verified by a 10-Gbps quadrature phase-shift keying (QPSK) CFSO transmission system.

II. Operation Principle of the Proposed Algorithm

A block diagram of the proposed scheme is shown in Fig. 1. The algorithm is divided into two stages. The first stage focuses on frame synchronization. The objective is to extract the timing training sequence by identifying the starting point of each training period frame in the received sequence. The damage to signal r_k (one sample per symbol) entering the carrier-phase recovery module was mainly due to carrier-phase errors caused by frequency deviations between the transmitter laser and the local oscillator (LO) laser and the LO laser linewidth and atmospheric turbulence and ASE noise. Other damages were assumed to be compensated by the previous clock synchronization and equalization modules; thus, the timing training symbols can maintain good correlation, and it is feasible to use the Park [27] timing synchronization algorithm to identify the starting point of the training symbols. A schematic diagram of the training sequence in one training period is shown in Fig. 2, where $[A_{N/4}B_{N/4}A^*_{N/4}B^*_{N/4}]$ denotes the timing training symbols in one period, and B is the symmetric sequence of A. The main idea is to use the correlation of the conjugate symmetric blocks of timed training symbols to determine the starting point of each training period frame in the received sequence. In the receiver, the timing metric can be calculated as follows:

$$M\left(d\right)=\frac{\left|\sum_{m=0}^{N/2-1}\left[r\left(d+m\right)r\left(d-m\right)\right]\right|^2}{\left(\sum_{m=0}^{N/2-1}\left|r\left(d+m\right)\right|^2\right)^2},M\left(d\right)\in\left[0,1\right] \tag{1}$$

where,

$$P\left(d\right)=\sum_{m=0}^{N/2-1}\left[r\left(d+m\right)r\left(d-m\right)\right] \tag{2}$$

$$R\left(d\right)=\sum_{m=0}^{N/2-1}\left|r\left(d+m\right)\right|^2 \tag{3}$$

where N denotes the training symbol length for one training period, $r(d)$ is the received sequence, and d is the time indicator of the received sequence. When $M(d)$ reaches its maximum value, the corresponding d denotes the location of the timing starting point. A block diagram of the maximum timing metric calculation is shown in Fig. 3.

The second stage is the FOE stage. After the starting position of the timing training symbols is found, the identified timing training symbols $R(k)$ (including $[A_{N/4}{}'B_{N/4}{}'A^*_{N/4}{}'B^*_{N/4}{}']$) are used for carrier FOE. Atmospheric turbulence can cause amplitude and phase disturbances in the optical signal in the channel. As discussed in [28], when only the phase of the symbol is considered, the received sequence can be expressed as follows:

$$R(k)=\exp\left[j\left(\begin{array}{l}\theta_s\left(k\right)+2\pi\Delta f_{est}kT\\+\theta_L\left(k\right)+\theta_c\left(k\right)+\theta_n\left(k\right)\end{array}\right)\right] \tag{4}$$

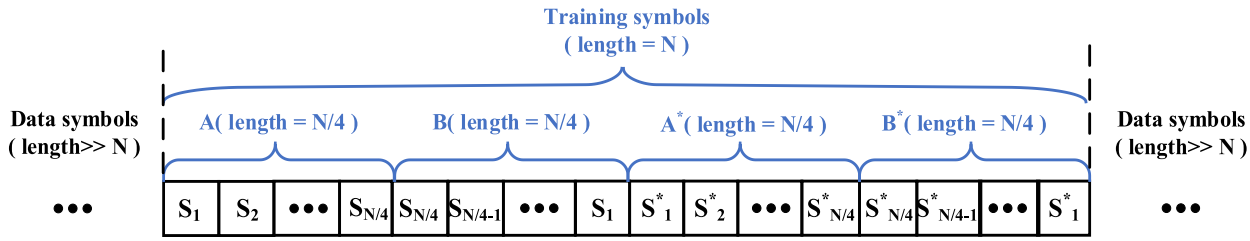

Fig. 2. Training symbols structure in one training period.

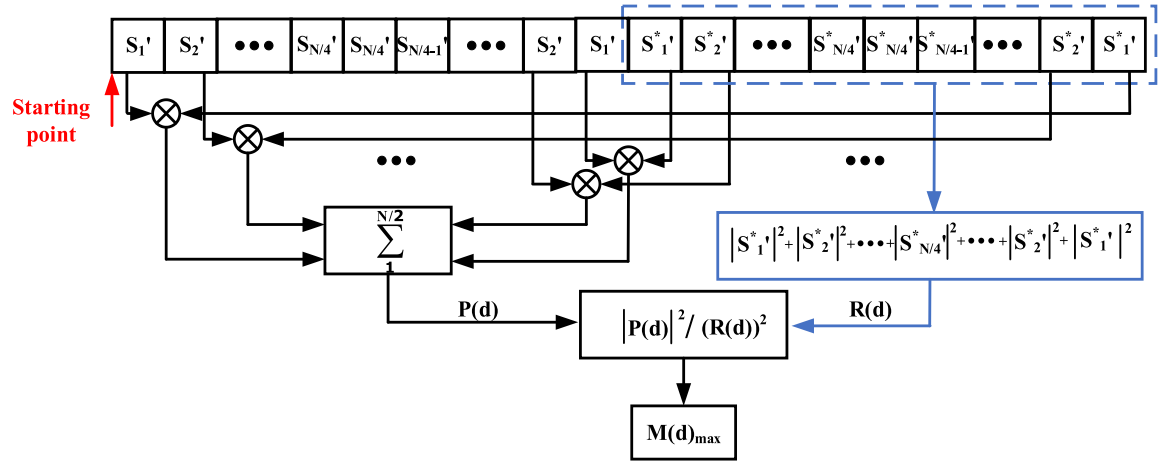

Fig. 3. Block diagram of the maximum timing metric calculation.

where $\theta_s(k)$ denotes the modulated phase information carried by the current signal, $2\pi\Delta f_{est}kT$ denotes the phase error caused by the carrier frequency offset of the kth training symbol, $\theta_L(k)$ denotes the phase noise caused by the LO laser linewidth, $\theta_c(k)$ denotes the phase noise introduced by atmospheric turbulence, and $\theta_n(k)$ denotes the ASE phase noise caused by the amplifier, which presents a zero-mean Gaussian distribution. The FOE operational flow of the second stage is indicated by the black dotted line in Fig. 1. It is worth noting that $\hat{R}(k)$ is the symmetric sequence of the original training sequence with a sequence structure. We first remove the signal modulation phase of the training symbols:

$$S(k) = R(k) \cdot \hat{R}(k) \tag{5}$$

Then, the phase error estimate caused by the frequency offset is easy to calculate:

$$2\pi\Delta f_{est}T = \arg\left[\sum_{N} S(k) \cdot S^{*}(k-1)\right] \tag{6}$$

where $T$is the symbol period, N is the number of training symbols $R(k)$, and $2\pi\Delta f_{est}T$represents the estimated frequency offset. The theoretical frequency offset estimated from the algorithm is $\pm 1/2T$, which is independent of the signal modulation format and omits the 4th power operations. Finally, the estimation result $2\pi\Delta f_{est}T$ can be used to correct the frequency offset present in the data symbols of a training period. It should be noted that the random fluctuations in the amplitude and phase of the received signal caused by changes in the refractive index due to atmospheric turbulence generally have frequencies between 20 Hz and 1 kHz [29], [30]. In a CFSO transmission system with a communication rate on the order of GHz, the phase noise variation caused by the LO laser linewidth and atmospheric turbulence varies relatively slowly, and its influence of two adjacent symbols can be considered the same [4], [29].

It is worth noting that the signal entering the carrier FOE module removes the signal damage caused by the sampling clock offset with a clock synchronization module. With a fixed training period, after the training symbols are localized in the first training period, the subsequent training periods do not require the localization computation of the Park algorithm, so the computational complexity of the timing synchronization part of this algorithm can be ignored. Table I shows a comparison of the hardware complexity of the FOE stage of various algorithms. Since the modulation format in the simulation is QPSK, the 4th power algorithm and FFT algorithm are used for comparison and analysis with the proposed algorithm, and their complexity is mentioned in [31]. N is the length of the training sequence block and the number of points in the FFT algorithm. Based on Table I and Equation (6), in the FOE stage, when compared with the 4th power and FFT algorithms, the proposed algorithm avoids the 4th power operation in the time domain and FFT in the

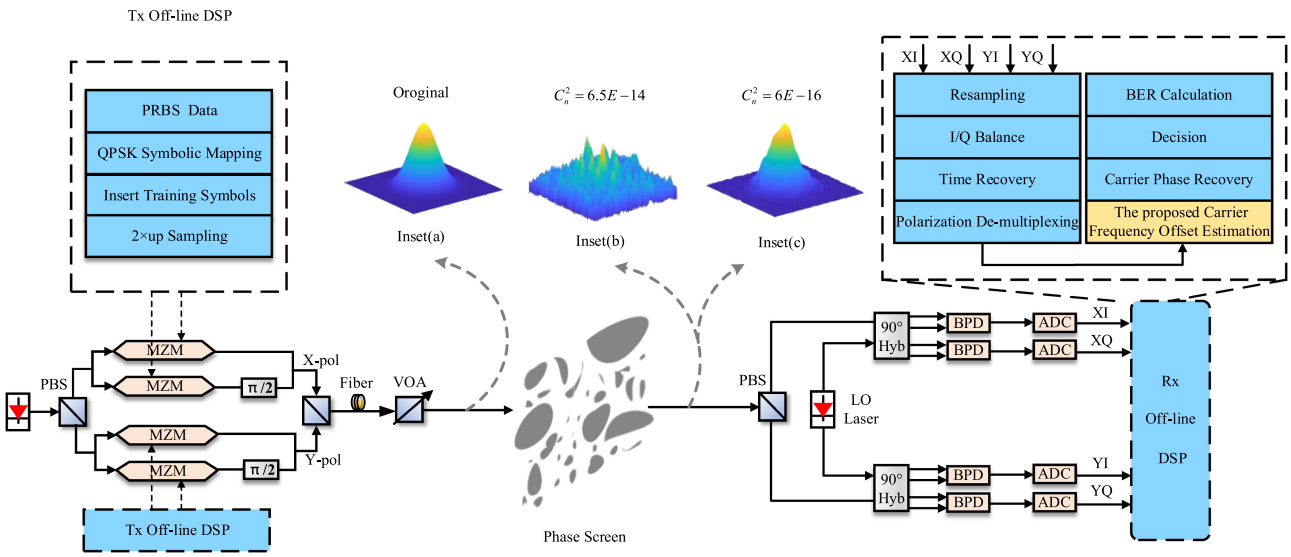

Fig. 4. Simulation setup for a 10-Gbps QPSK transmission system.

TABLE I
COMPUTATIONAL COMPLEXITY OF DIFFERENT SCHEMES

Scheme	Real Multiplications	Real Additions
FFT Algorithm	$8N+2Nlog_2N+2$	$4N+3Nlog_2N$
4th Power Algorithm	$12N+2$	$8N-2$
STSB Algorithm	$8N$	$6N-2$

frequency domain, which reduces the computational complexity of the algorithm and helps to reduce the complexity of the whole scheme.

III. SIMULATION DEMONSTRATION AND PERFORMANCE EVALUATION

To evaluate the performance of the proposed STSB carrier frequency offset estimation scheme, a 10-Gbps QPSK CFSO simulation platform was constructed based on MATLAB simulation tools, as shown in Fig. 4. The black dotted line depicts the typical DSP flows at Tx and Rx for a CFSO communication system. At the Tx DSP, the training symbols and data symbols are provided by a pseudorandom bit sequence (PRBS) generated by the same MATLAB program. The training symbols for the frame synchronization were inserted into the signal to be transmitted before the electronic-to-optical conversion. After that, an external cavity laser (ECL) with a linewidth of 50 kHz was divided into two orthogonally polarized light signals using a polarization beam splitter (PBS); two dual parallel Mach-Zehnder modulators were used to modulate the two orthogonally polarized light signals, and the four discrete data signals generated correspond to the real and imaginary parts of the X and Y polarization states, respectively. The optical signals of the two output polarization states were combined by a polarization beam combiner (PBC) and integrated into a computer-simulated free-space turbulent channel. A variable optical attenuator (VOA) was used to simulate different transmitting powers at the transmitter side. At the receiver, the received optical fields were mixed with a local oscillator (LO) laser and detected by balanced photodiodes (BPDs). In addition, the linewidth of the LO laser was set to 50 kHz and has 300 MHz frequency offset with transmitter laser. Finally, the signal was sampled by an analog-to-digital converter (ADC) and subsequently processed by the Rx DSP algorithm. The Rx DSP algorithm includes compensation for the in-phase/quadrature (I/Q) balance, timing recovery, polarization demultiplexing, the STSB carrier FOE, carrier phase recovery (CPR), the decision, and the BER calculation.

This study used the classic McGlamery's phase screen model of atmospheric turbulence based on the active power spectrum, which uses two-dimensional Fourier transform technology to simulate the atmospheric turbulence phase disturbances [32]. Because the atmospheric turbulence occurred within a range of approximately 10 km at the ground level, the simulation platform was configured with an atmospheric turbulence range of z = 10 km. The internal scale of the atmospheric turbulence was negligible, while the external scale was infinite. In addition, we set λ (wavelength) equal to 1550 nm, and the parameters of the atmospheric refractive index structure C_n^2 were set to $6E-16m^{-2/3}$ and $6.5E-14m^{-2/3}$ (these are two types of classic atmospheric refractive index structural parameters that correspond to weak and strong turbulent atmospheric channels) [30]. The three-dimensional intensity distributions of the Gaussian beam under different atmospheric turbulence conditions are shown in insets (a, b, c) in Fig. 4.

For the TSB algorithm, it is essential to achieve precise recognition of the training sequence. Fig. 5 shows the timing metrics $M(d)$ of different transmitting powers under strong and weak turbulence conditions with a frequency offset of 300 MHz. The results indicate that the timing synchronization algorithm can correctly identify the starting position of the training sequence under both strong and weak turbulence. In

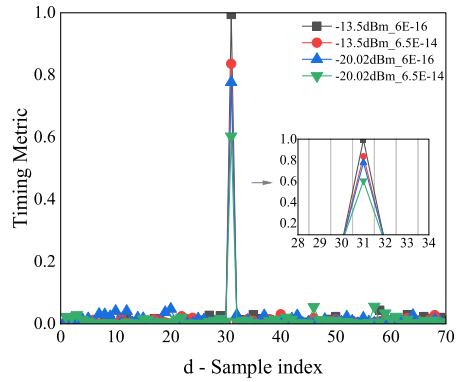

Fig. 5. Timing metric function with different transmitting powers.

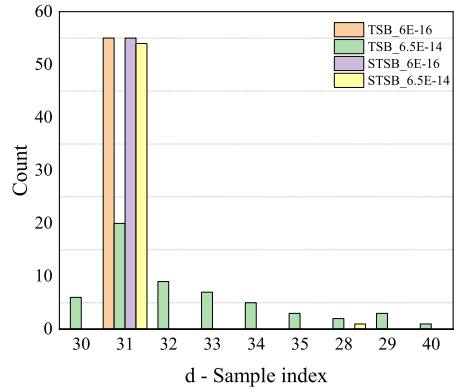

Fig. 6. Timing metric function under 55 random phases.

addition, the synchronization algorithm was still effective when the transmitting power was low. A clear difference between the threshold value at the peak and the adjacent values can result in a sharp pulse-shaped timing measurement curve, and the peak of the timing measurement function decreases as the transmitting power decreases. In addition, Fig. 6 compares the accuracy of the timing synchronization of 55 phase grayscale images in the same turbulence state under the same low transmitting power (-22 dBm) between the proposed STSB scheme and TSB scheme. As shown in Fig. 6, at the same low transmitting power, the probability of timing error of the proposed STSB algorithm was much lower than that of TSB algorithm. Compared with the SC-based TSB algorithm, the proposed STSB algorithm greatly avoids the increase in BER caused by timing inaccuracies at low transmitting power. In this simulation, the training sequence began with the 31st symbol and the length of the timing training symbol block N is 256.

On this basis, we compared the normalized mean square error (MSE) of the QPSK system with the symbol block length N and the transmitting power in strong and weak turbulence channels. We also compared the proposed algorithm with the 4th power algorithm, as shown in Fig. 7. Fig. 7 shows that the FOE accuracy of both algorithms increased as the number of symbols involved in the FOE operation and the optical power at the transmitter increased. When the number of symbols was

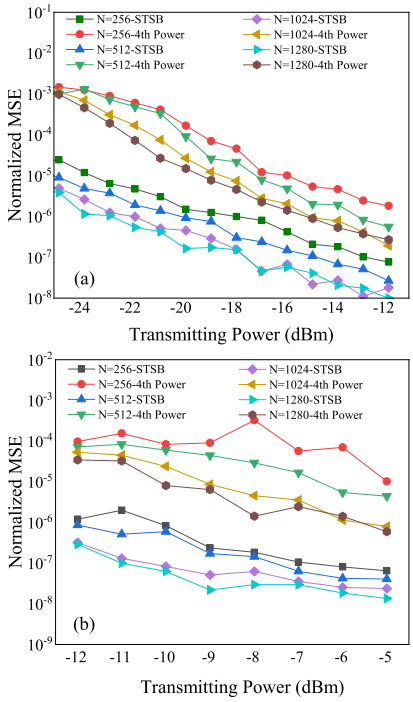

Fig. 7. Normalized MSE as a function of the transmitting power for different values of N, with C_n^2 equal to (a) $6E-16m^{-2/3}$ and (b) $6.5E-14m^{-2/3}$.

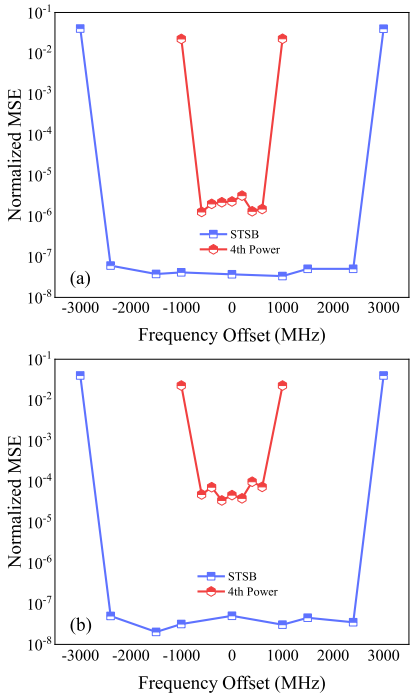

Fig. 8. Normalized MSE as a function of different frequency offsets with C_n^2 equal to (a) $6E-16m^{-2/3}$ and (b) $6.5E-14m^{-2/3}$.

small, the FOE accuracy was greatly affected by the turbulence intensity. However, the proposed STSB algorithm performed significantly better than the 4th power algorithm with fewer symbol blocks and provided more accurate frequency offset estimates. Considering the effects of noise tolerance, frequency

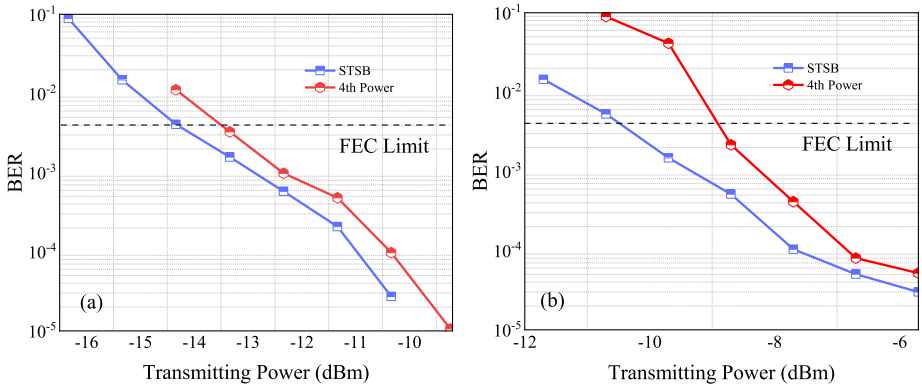

Fig. 9. BER as a function of the transmitting power at different N values for the proposed algorithm with C_n^2 equal to (a) $6E-16m^{-2/3}$ and (b) $6.5E-14m^{-2/3}$.

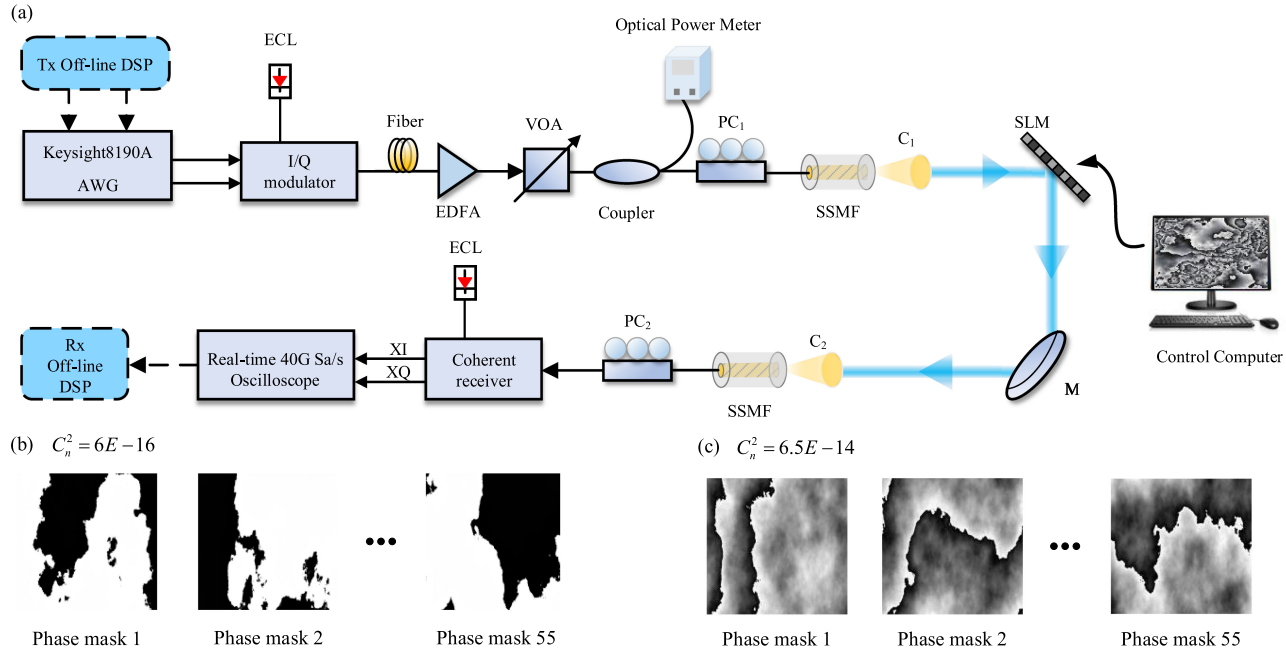

Fig. 10. (a) Experimental setup for a 10-Gbps QPSK transmission system under different turbulence channels. Grayscale image under different refractive index structural parameters: (b) $6E-16m^{-2/3}$ and (c) $6.5E-14m^{-2/3}$. PC: polarization controller, C: collimator, M: mirror, SLM: space light modulator.

offset tracking, and computational overhead [33], the length N of the training symbol block was set to 1024 in the simulation.

In Fig. 8, the normalized MSE of the algorithm at different frequency offsets under strong and weak turbulence conditions are compared with those of the 4th power algorithm. Here, the number of training symbols (N) for both algorithms was set to 1024. The transmitting power values of the strong and weak turbulence states were -10.5 dBm and -15dBm, respectively. According to Fig. 8, the estimated values of the proposed algorithm in this study were more accurate, with lower normalized MSE and more advantageous under strong turbulence. Since the proposed algorithm avoids the 4th operation to remove the modulated phase in the FOE phase, the FOE range was approximately four times that of the traditional 4th power algorithm.

Fig. 9 shows the proposed STSB scheme with the 4th algorithm in terms of transmitting power as a function of BER under different atmospheric turbulence channels. The simulation system set the frequency offset to 300MHz and the length of the FOE symbol block was 1024. As shown in Fig. 9, when the FEC threshold was 3.8×10^{-3}, the sensitivity of the STSB carrier FOE scheme was improved by about 1.92 dB and 1.2 dB for the strong and weak turbulence channels, respectively.

IV. Experimental Setup and Results

To further investigate the performance of the proposed algorithm, 10-Gbps QPSK CFSO communication experiments were conducted under different atmospheric turbulence conditions; the experimental setup is shown in Fig. 10(a). A PLUTO-2 phase-type space optical modulator (SLM) from HOLOEYE was used to simulate the turbulence channel at a resolution of 1920 $\times$ 1080 pixels [34], [35]. Because existing commercial

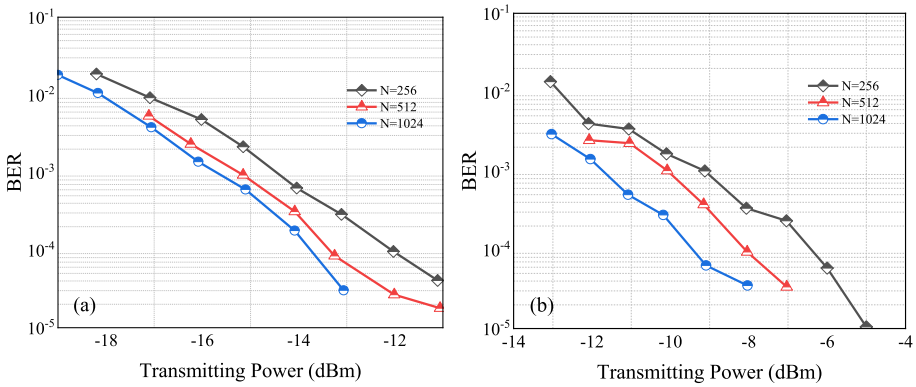

Fig. 11. Experimentally measured BER as a function of the transmitting power at different N values for the proposed algorithm with C_n^2 equal to (a) $6E-16m^{-2/3}$ and (b) $6.5E-14m^{-2/3}$.

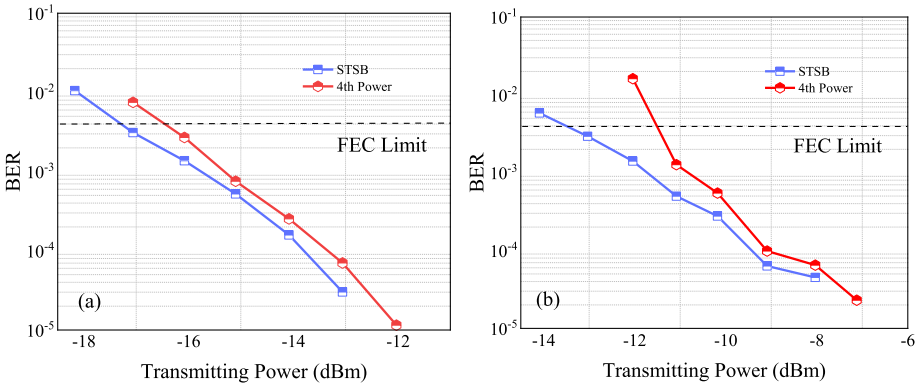

Fig. 12. Experimentally measured BER as a function of the transmitting power for the proposed algorithm and the 4th power algorithm with C_n^2 equal to ($N=1024$) (a) $6E-16m^{-2/3}$ and (b) $6.5E-14m^{-2/3}$.

SLMs are polarization-sensitive, it is difficult to achieve polarization multiplexing in experiments. However, the polarization damage caused by atmospheric turbulence is small and can be compensated for by channel equalization. The proposed algorithm mainly focuses on signal phase changes, which are independent of the polarization state; thus, a single-polarization state experiment can also be used to verify the performance of the proposed algorithm. In the experiment, the SLM consisted of a driver circuit and a liquid crystal (LC) screen. The driver circuit was connected to a control computer that generated grayscale images according to the different parameters of the atmospheric refractive index structure C_n^2 and loaded them onto the LC of the SLM. For each atmospheric turbulence state, about 55 random different phase masks were generated and converted to grayscale images, as shown in Fig. 10(b) and (c).

The same MATLAB procedures as in the simulation were used in the transmitter to generate the data symbols. Subsequently, the corresponding I and Q modulated components were sent to the Keysight arbitrary waveform generator (AWG) M8190A, which drove the IQ modulator to generate the modulated optical signal. The IQ modulator has an integrated tunable external cavity laser with a measured linewidth of 50 kHz. The optical signal was then passed through the transmitting lens after it was enhanced by an erbium-doped optical fiber amplifier (EDFA). The optical transmitting power was varied within a certain range by adjusting the VOA control. After the polarization controller PC_1 and the collimator C_1, the signal beam propagated in free space with the polarization direction same as the function direction of SLM. The signal beam reached the receiver side after reflected by SLM, mirror M, and passed through the collimator C_2. At the receiver side, polarization PC_2 controlling was performed at first. Then, the received signal was connected to the coherent receiver and the oscilloscope. The operating wavelength of the LO laser was 193.400 THz, and the linewidth was 50 kHz. With a stable central wavelength, the frequency offset between the transmitting laser and the LO laser was about 300 MHz. The whole indoor link distance is 900 mm. The laser beam wavelength is 1550 nm. Collimators C_1-C_2 are the same and the focal length is 11.29 mm. So, the diameter of transmitting beam D is 2.1 mm. According to Fresnel scaling theory, the experimental setup can be equivalent to outdoor long-distance experiments [36]. In addition, the clock of this experiment was synchronized with the clock source of the AWG and the oscilloscope.

Fig. 11 shows the BER curves of the proposed algorithm vs. the symbol block length N and the optical transmitting power for

the 10-Gbps QPSK CFSO communication system in different turbulence states. The experiments show that the performance of the algorithm decreases with the number of training symbol blocks in different turbulence states and has a low BER when the number of symbol blocks N is 1024, which is consistent with the simulation results. The length of the training symbol block was set to 1024 in the experiment. For further comparison with the conventional 4th power algorithm, we generated transmitting power vs. BER curves for different atmospheric turbulence conditions, as shown in Fig. 12. When the FEC threshold was 3.8×10^{-3}, the sensitivity of the STSB carrier FOE scheme was 1.9 dB and 1 dB higher than that of the traditional 4th power algorithm under strong and weak turbulence conditions, respectively. The experiments show that the proposed scheme significantly increases the sensitivity of the receiver. In addition, there is a difference of nearly 3 dB between the experimental and simulated results owing to the lack of polarization multiplexing in the experiment. It can thus be seen that the conclusions drawn from the experiments and simulations are approximately the same.

V. Conclusion

In this article, a STSB carrier frequency offset estimation scheme for CFSO communication in QPSK modulation was proposed. A symmetric training sequence was developed to accurately identify the correct temporal position of a data frame based on received atmospheric signals. The simulation results demonstrate that high timing synchronization accuracy can be achieved even at low transmitting powers. Additionally, the proposed algorithm can achieve high-accuracy carrier FOE with less complexity and fewer frequency offset estimated symbol blocks in the FOE range of $\pm$ symbol rate/2. The simulated results show that, compared with the 4th power algorithm, the optical transmitting power required to reach the FEC threshold (3.8×10^{-3}) using the proposed algorithm was reduced by 1.92 dB and 1.2 dB for the strong and weak turbulence channels, respectively. The experimental results further verified the robustness and feasibility of the proposed scheme for QPSK CFSO communication transmission. In addition, the improvements of receiver sensitivity have been also experimentally validated.

Acknowledgment

The authors would like to thank Wuxi Electric Power Supply Company.

References

[1] H. Kaushal and G. Kaddoum, "Optical communication in space: Challenges and mitigation techniques," *IEEE Commun. Surv. Tut.*, vol. 19, no. 1, pp. 57–96, Jan.–Mar. 2017, doi: 10.1109/COMST.2016.2603518.

[2] A. K. Majumdar, *Advanced Free Space Optics (FSO): A Systems Approach*. Springer, 2014.

[3] H. Kaushal, V. K. Jain, and S. Kar, *Free Space Optical Communication*. 1st ed. Springer, 2017.

[4] L. C. Andrews, *Laser Beam Propagation Through Random Media*, vol. 99, 2nd ed. WA, USA: SPIE, 2001.

[5] M. Toyoshima, T. Takahashi, and K. Suzuki, "Results from phase-1, phase-2 and phase-3 kirari optical communication demonstration experiments with the NICT optical ground station (KODEN)," in *Proc. 25th AIAA Int. Commun. Satell. Syst. Conf.*, 2007, Art. no. 3228.

[6] J. Kovalik, A. Biswas, and K. Wilson, "Data products for the OCTL to OICETS optical link experiment," *Int. Soc. Opt. Eng.*, vol. 7587, 2010, Art. no. 75870.

[7] M. Yoshida, T. Hirooka, K. Kasai, and M. Nakazawa, "Single-channel 40 Gbit/s digital coherent QAM quantum noise stream cipher transmission over 480 km," *Opt. Exp.*, vol. 24, no. 1, pp. 652–661, Jan. 2016, doi: 10.1364/OE.24.000652.

[8] M. Morsy-Osman *et al.*, "DSP-free 'coherent-lite' transceiver for next generation single wavelength optical intra-datacenter interconnects," *Opt. Exp.*, vol. 26, no. 7, pp. 8890–8903, Apr. 2018, doi: 10.1364/OE.26.008890.

[9] T. Y. Elganimi, "Performance comparison between OOK, PPM and pam modulation schemes for free space optical (FSO) communication systems: Analytical study," *Intern. J. Comp. App.*, vol. 79, no. 11, pp. 22–27, Oct. 2013.

[10] M. L. B. Riediger, R. Schober, and L. Lampe, "Blind detection of on-off keying for free-space optical communications," in *Proc. Can. Conf. Elect. Comput. Eng.*, 2008, pp. 1361–1364.

[11] Z. Haijun, X. Weilin, Z. Ling, B. Yuanshuo, W. Wei, and D. Yi, "Performance analysis of FSO coherent BPSK systems over rician turbulence channel with pointing errors," *Opt. Exp.*, vol. 27, no. 19, pp. 27062–27075, Sep. 2019, doi: 10.1364/OE.27.027062.

[12] L. Siao and H. Hao, "Enabling technology in high-baud-rate coherent optical communication systems," *IEEE Access*, vol. 8, pp. 111318–111329, Jun. 2020, doi: 10.1109/ACCESS.2020.3003331.

[13] C. Jingtai, Z. Xiaohui, L. Wei, and G. Haijun, "Performance analysis of a coherent free space optical communication system based on experiment," *Opt. Exp.*, vol. 25, no. 13, pp. 15299–15312, Jun. 2017, doi: 10.1364/OE.25.015299.

[14] N. Mingbo, S. Xuegui, and C. Julian, "Performance analysis of coherent wireless optical communications with atmospheric turbulence," *Opt. Exp.*, vol. 20, no. 6, pp. 6515–6520, Mar. 2012, doi: 10.1364/OE.20.006515.

[15] W. Meng, Z. Huiying, and C. Baiquan, "PS-QPSK modulation system analysis in FSO," *Res. Exploration Lab.*, vol. 36, no. 4, pp. 146–183, Apr. 2017.

[16] W. Zixiong, Z. Wende, and S. Nianfu, "Performance comparison of different modulation formats over free-space optical (FSO) turbulence links with space diversity reception technique," *IEEE Photon. J.*, vol. 1, no. 6, Dec. 2009, doi: 10.1109/JPHOT.2009.2039015.

[17] M. A. Esmail, "Experimental performance evaluation of weak turbulence channel models for FSO links," *Opt. Commun.*, vol. 486, Jan. 2021, Art. no. 126776, doi: 10.1016/j. optcom.2021.126776.

[18] K. Xizheng, W. Jiali, and Y. Shangjun, "Research progress and prospect of atmospheric turbulence for wireless optical communication," *Chin. J. Radio Sci.*, vol. 36, no. 3, pp. 323–339, Jun. 2021, doi: 10.12265/j. cjors.2020116.

[19] A. Bhattacharjee and A. K. Jha, "Experimental demonstration of structural robustness of spatially partially coherent fields in turbulence," *Opt. Lett.*, vol. 45, no. 14, pp. 4068–4071, Jul. 2020, doi: 10.1364/OL.395697.

[20] F. Nadeem, V. Kvicera, M. S. Awan, E. Leitgeb, S. S. Muhammad, and G. Kandus, "Weather effects on hybrid FSO/RF communication link," *IEEE J. Select. Areas Commun.*, vol. 27, no. 9, pp. 1687–1697, Dec. 2009, doi: 10.1109/JSAC.2009.091218.

[21] C. Jingchi *et al.*, "Relative phase noise estimation and mitigation in raman amplified coherent optical communication system," *Opt. Exp.*, vol. 22, no. 2, pp. 1257–1266, Jan. 2014, doi: 10.1364/OE.22.001257.

[22] M. Selmi, Y. Jaouën, and P. Ciblat, "Accurate digital frequency offset estimator for coherent pol mux QAM transmission systems," in *Proc. 35th Eur. Conf. Opt. Commun.*, 2009, pp. 1–2.

[23] L. Jianing, W. Qiong, and J. Hexun, "Efficient timing/frequency synchronization based on sparse fast Fourier transform," *J. Lightw. Technol.*, vol. 37, no. 20, pp. 5299–5308, Oct. 2019, doi: 10.1109/JLT.2019.2932075.

[24] A. Leven, N. Kaneda, and U. V. Koc, "Frequency estimation in intradyne reception," *IEEE Photon. Technol. Lett.*, vol. 19, no. 6, pp. 366–368, Dec. 2006, doi: 10.1109/LPT.2007.891893.

[25] Z. Xian, C. Xue, and L. Keping, "Wide-range frequency offset estimation algorithm for optical coherent systems using training sequence," *IEEE Photon. Technol. Lett.*, vol. 24, no. 1, pp. 82–84, Jan. 2011, doi: 10.1109/LPT.2011.2172790.

[26] T. M. Schmidl and D. C. Cox, "Robust frequency and timing synchronization for OFDM," *IEEE Trans. Commun.*, vol. 45, no. 12, pp. 1613–1621, Dec. 1997.

[27] B. Park, H. Cheon, and C. Kang, "A novel timing estimation method for OFDM systems," *IEEE Commun. Lett.*, vol. 7, no. 5, pp. 239–241, May 2003, doi: 10.1109/LCOMM.2003.812181.

[28] L. Xueliang, G. Tianwen, and M. Shuang, "Performance improvement of coherent free-space optical communication with quadrature phase-shift keying modulation using digital phase estimation," *Appl. Opt.*, vol. 56, no. 16, pp. 4695–4701, May 2017, doi: 10.1364/AO.56.004695.

[29] Z. Xiaoxin, Z. Zeyu, T. Peng, and Y. Xiuhua, "Numerical research on partially coherent flat-topped beam propagation through atmospheric turbulence along a slant path," *Appl. Opt.*, vol. 58, no. 34, pp. 9443–9454, Dec. 2019, doi: 10.1364/AO.58.009443.

[30] L. C. Andrews, *Laser Beam Scintillation With Applications*. SPIE Press, 2001.

[31] A. Meiyappan, P. Kam, and H. Kim, "On decision aided carrier phase and frequency offset estimation in coherent optical receivers," *J. Lightw. Technol.*, vol. 31, no. 13, pp. 2055–2069, Jul. 2013, doi: 10.1109/JLT.2013.2260723.

[32] J. D. Schmidt, *Numerical Simulation of Optical Wave Propagation with Examples in MATLAB*. Bellingham, WA, USA: SPIE, 2010.

[33] G. Goldfarb and L. Guifang, "BER estimation of QPSK homodyne detection with carrier phase estimation using digital signal processing," *Opt. Exp.*, vol. 14, pp. 8043–8053, 2006.

[34] Q. Zhen and I. B. Djordjevic, "Approaching terabit optical transmission over strong atmospheric turbulence channels," in *Proc. 18th Int. Conf. Trans. Opt. Netw.*, 2016, pp. 1–5, doi: 10.1109/ICTON.2016.7550346.

[35] C. Shanyong, Z. Zhiguo, and H. Yang, "Demonstration of turbulence and pointing error resistant for free-space to single-mode coupling using photonic lantern," in *Proc. 24th OptoElect. Commun. Conf. Int. Conf. Photon. Switching Comput.*, 2019, pp. 1–3.

[36] B. Rodenburg, M. Mirhosseini, and M. Malik, "Simulating thick atmospheric turbulence in the lab with application to orbital angular momentum communication," *New J. Phys.*, vol. 16, no. 3, Aug. 2014, Art. no. 33020, doi: 10.1088/1367-2630/16/8/089501.